ADVANCED FUNCTIONAL MATERIALS
www.afm-journal.de

Insulator-Conductor Type Transitions in Graphene-Modified Silver Nanowire Networks: A Route to Inexpensive Transparent Conductors

*Izabela Jurewicz, Azin Fahimi, Phillip E. Lyons, Ronan J. Smith, Maria Cann, Matthew L. Large, Mingwen Tian, Jonathan N. Coleman, and Alan B. Dalton**

Silver nanowire coatings are an attractive alternative to indium tin oxide for producing transparent conductors. To fabricate coatings with low sheet resistance required for touchscreen displays, a multi-layer network of silver nanowires must be produced that may not be cost effective. This problem is counteracted here by modifying the electrical properties of an ultra-low-density nanowire network through local deposition of conducting graphene platelets. Unlike other solution-processed materials, such as graphene oxide, our pristine graphene is free of oxygen functional groups, resulting in it being electrically conducting without the need for further chemical treatment. Graphene adsorption at inter-wire junctions as well as graphene connecting adjacent wires contributes to a marked enhancement in electrical properties. Using our approach, the amount of nanowires needed to produce viable transparent electrodes could be more than 50 times less than the equivalent pristine high density nanowire networks, thus having major commercial implications. Using a laser ablation process, it is shown that the resulting films can be patterned into individual electrode structures, which is a pre-requisite to touchscreen sensor fabrication.

1. Introduction

The vast majority of today's touchscreen devices, such as smart phones and tablets, use indium tin oxide (ITO) deposited on either glass or plastic films as the active material. ITO is processed using high temperature vacuum deposition, which makes the manufacturing process very expensive. There is also a drive to replace ITO because of limited global availability and price concerns. In addition, ITO is relatively brittle so may not be considered the material of choice for applications where the development of exceptionally large curved screens, bendable smart displays and wearable devices are driving market interest. To meet the increase in demand for an alternate transparent conducting material, coatings containing ensembles of silver nanowires (AgNWs) are being put forward as a cost-effective and sustainable alternative to ITO.[1–9]

Key challenges associated with the fabrication of AgNW based transparent conductors such as time evolving oxidation,[10] weak adhesion to substrates,[7,11] and haze[12–14] are already being resolved. Recently, it has been demonstrated that AgNW based conductors possess higher transparency at equivalent ITO sheet resistance values. However, despite the obvious promise there is need for improvement. The inherent junction resistance associated with electron transport between wires is one of the major limiting factors on the electrical conductivity of percolating assemblies of AgNWs. Although this may be overcome by welding at overlapping junctions,[15–17] such temperature treatment could damage certain substrates and also represents an expensive post-fabrication process.

Another possibility is to combine AgNWs with other nanostructured materials such as CNTs[18,19] or graphene to form hybrid coatings.[10,20–24] For instance, by using capillary forces during solvent evaporation of graphene oxide (GO) dispersions, followed by thermal annealing, Yun et al.[21] made flexible and mechanically robust GO/AgNW hybrids with a transmittance of ca. 86% and a sheet resistance $R_s \approx 150\ \Omega$/sqr. Dip coating has also been used to deposit reduced graphene oxide (rGO) onto a AgNW network resulting in a highly conducting ($R_s \approx 50\Omega$/sqr) and transparent hybrid electrode material.[10] The most common material to form a hybrid structure with is polycrystalline graphene grown by Chemical Vapor Deposition (CVD).[22–25] Kholmanov et al.[22] used a modified dry transfer process to apply CVD grown graphene onto AgNW

Dr. I. Jurewicz, Dr. A. Fahimi, M. Cann, M. L. Large, Dr. A. B. Dalton
Department of Physics
Faculty of Engineering and Physical Sciences
University of Surrey
Guildford GU2 7XH, UK
E-mail: a.dalton@surrey.ac.uk
Dr. P. E. Lyons, R. J. Smith, Prof. J. N. Coleman
School of Physics
Trinity College Dublin
Dublin, Ireland
M. Cann
M-Solv Ltd, Oxonian Park
Langford Locks
Kidlington, Oxfordshire, UK
Dr. M. Tian
NT-MDT Europe B. V.
High Tech Campus 83
5656 AG, Eindhoven, The Netherlands

DOI: 10.1002/adfm.201402547

films resulting in a T above 90% and an R_s = 64 Ω/sqr. In other work AgNW ink was drop cast before or after transfer of CVD grown graphene onto a substrate with a result of T = 88% and R_s = 22 Ω/sqr.[23] A hot-pressing method has also been used to transfer CVD grown graphene onto AgNWs.[24] Resulting films have T>90% and R_s = 14 Ω/sqr. All the above studies indicate that there is potential for using hybrid systems of nanowires and graphene to produce transparent electrode structures that are comparably better than ITO. However, there are fundamental limitations in terms of commercial viability. Most of the work has relied on graphene grown by CVD. Presently, this is an expensive process that normally requires high temperature growth followed by complicated post processing. Moreover, as of today, there are still issues in the realization of CVD as a scalable process to produce high quality graphene in commercially viable quantities.

In this report, we show a simple, scalable and relatively inexpensive method to prepare highly conducting AgNW/graphene hybrid transparent electrodes employing low-cost solution-processed pristine graphene. Unlike other solution-processed materials such as GO, our pristine graphene is free of oxygen functional groups resulting in it being electrically conducting without the need for further chemical treatment. We use a combination of spray deposition and Langmuir-based techniques[26] to produce ultrathin films with controlled nanowire and graphene densities. We demonstrate that adsorption of graphene at nanowire junctions markedly effects the macroscopic conductivity without significantly reducing the optical transmittance. Our optimized films, which have comparable properties to commercial ITO, therefore contain reduced levels of AgNWs in comparison to films made of pristine AgNWs with the same properties. We also show that the resulting films can be patterned using laser ablation at relatively low fluences to produce electrically isolated scribes suitable for touchscreen device fabrication. The results indicate that these graphene/nanowire hybrid films may serve as a cheap replacement for existing technologies in electronic devices.

2. Results and Discussion

Industrial scale applications of transparent AgNW films require the electrode material to be deposited promptly and cost effectively. For this reason we choose spray coating for the deposition of AgNWs. This technique allows for excellent control over a variety of parameters (pressure, flow rate, scans speed, nozzle distance from the sample surface, temperature of the substrate, etc.) to produce consistent and reproducible transparent coatings.[27,28] Samples of low, medium and high density AgNW networks were formed by varying the number of spray-passes that closely follow the transmittance vs sheet resistance (T vs R_s) dependence as shown by others, with the conductor network undergoing a transition from bulk-like to percolative behavior.[29,30] For ease of discussion the following abbreviations will be used L-AgNW, M-AgNW, H-AgNW to distinguish between low (R_s > 1 kΩ), medium (100 Ω < R_s < 1 kΩ), and high density (R_s < 100 Ω) AgNW networks respectively. As can be seen in **Figure 1**a, H-AgNW consists of more than 4 layers of wires, M-AgNW between 3–4 layers, and L-AgNW between 1–3 layers. All films are high quality, with no perceivable aggregates observed, producing minimal haze. The transmittance of all samples is between ca. 92 to ca. 98% (excl. glass) (**Figure 2**b) decreasing monotonically as the AgNWs density is increased and have all much higher transmittance than commercially available ITO.

As the AgNWs are randomly ordered on the substrate there is an isotropic distribution of wire-wire junctions, which as stated previously is one of the limiting factors on the electrical conductivity. As shown in Figure 1 using the L-AgNW sample as an example, we can use a combination of atomic force microscopy (AFM) and scanning spreading resistance microscopy (SSRM), measured concurrently, to investigate the physical connections between individual wires and the associated electrical properties at specific junctions. The representative AFM height image in Figure 1e shows wires lying on top of each other in intimate contact while forming an extended percolating network. After a bias voltage is applied to the AFM probe, measurements of local current flow through the sample are performed simultaneously with surface topography imaging.[31] As can be seen in the current flow distribution map in Figure 1f, AgNWs form connected networks with a significant out-of-plane and in-plane current flow. In a region where a nanowire has been deposited in such a way as to be isolated from the network it is clear that while it appears in the topography image it is not present in the SSRM image, as we would expect.

To fabricate AgNW/graphene hybrids, the Langmuir-Schaefer (LS) horizontal graphene deposition technique was used as described in the experimental section. Although a significant number of graphene flakes are single-layered, flakes consisting of two-layers, three layers and multilayers are also present in the dispersion. The average flake length is ca. 305 nm.[26] As a result of spreading the pristine graphene dispersion at the air-water interface, a Langmuir film of graphene is formed and subsequently compressed to reach a surface pressure of Π = 25 mN m^{-1} (Figure 2a). Throughout the compression, the graphene monolayer undergoes phase transitions (from gas-like to liquid-like to solid-like) yielding a pressure-area (density) (Π-A) isotherm as shown in Figure 2b. The LS horizontal deposition was used to transfer the formed graphene monolayers onto a substrate containing AgNW networks that were spray-deposited prior to graphene deposition. This was realized by lowering the substrate onto the graphene-covered interface. Once contact with the substrate was made, the substrate was retracted resulting in the graphene flakes being transferred onto the AgNWs via a capillary driven mechanism. As a control experiment, pristine AgNW films were also lowered directly onto the air water interface without graphene present. There was no difference in R_s of pristine AgNW films before and after this step indicating that the process itself does not significantly remove any AgNWs from the substrate during Langmuir-Schaefer deposition of graphene. Direct deposition of graphene onto a glass substrate at this surface pressure yields ca. 70% surface coverage and a corresponding T ≈ 85% as shown in Figure 2b. Similar results are obtained when graphene is deposited on the surface of a sprayed AgNWs film.

As can be seen in **Figure 3** b-d, although graphene is present everywhere, the majority of flakes preferentially locate on the AgNWs rather than on the substrate since the first contact

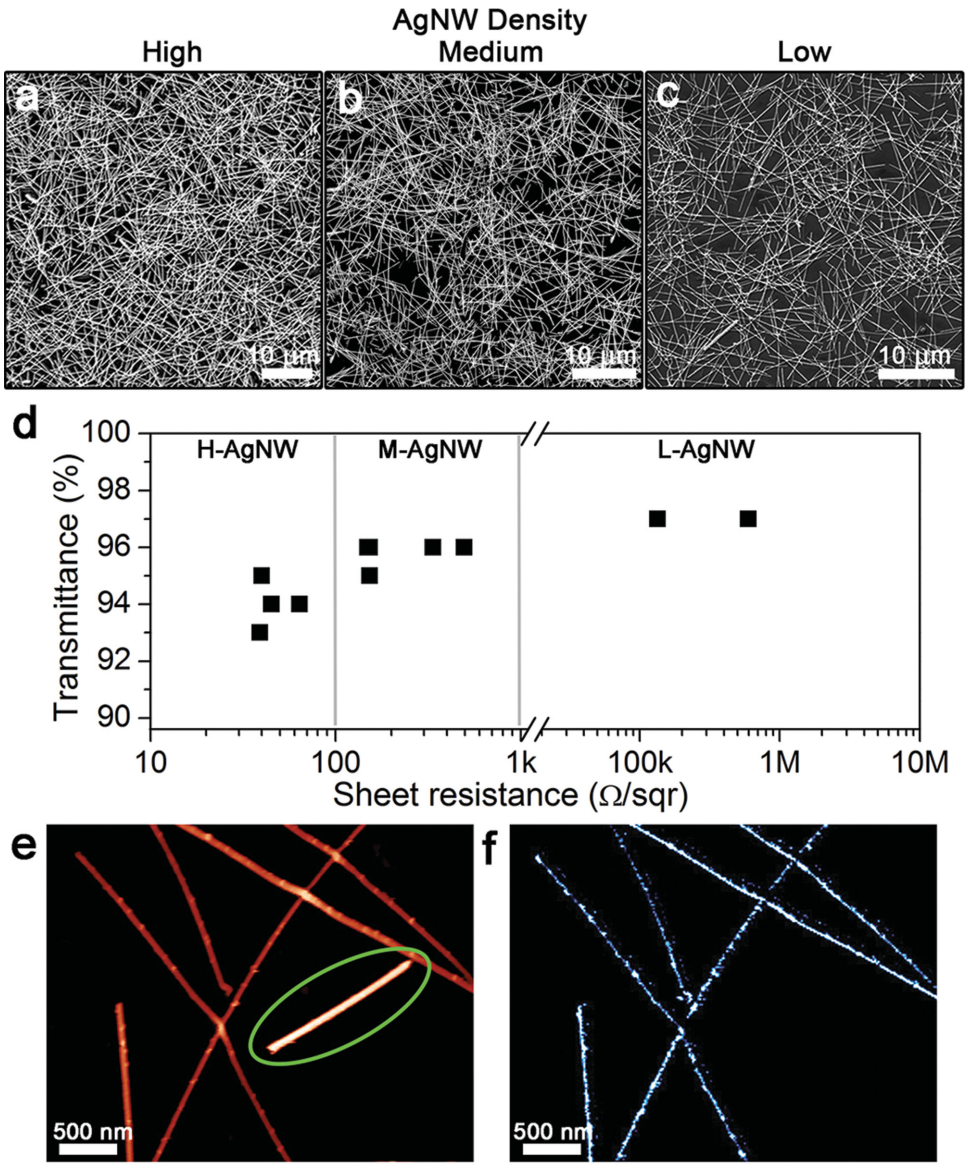

Figure 1. SEM images of spray-deposited AgNW networks on glass substrates as a function of AgNW density: a) high (H-AgNW), b) medium (M-AgNW), c) low (L-AgNW). d) Transmittance (@550 nm) plotted versus sheet resistance of AgNWs networks of various densities and high magnification e) AFM topography and corresponding f) SSRM surface conductivity map of L-AgNW. The black background represents no current flow, and white regions show a current flow on the order of nA (see Supporting Information Figure S1)

points during deposition is made on the wires. The R_s measured after deposition at $\Pi = 25$ mN m^{-1} improved by ca. 100% for the L-AgNW with ca. 80% and ca. 30% improvement being realized for M-AgNW and H-AgNW respectively. For example, the R_s = 8.9 MΩ/sqr (at 97% transmittance) of L-AgNW reduced to 4.9 kΩ/sqr and for H-AgNW the R_s dropped from 25 Ω/sqr (at 93% transmittance) to 19 Ω/sqr. The decrease in R_s is particularly marked where the nanowires are present at low densities. The smallest improvement in R_s is for dense networks as the graphene interacts only with the exterior layers of AgNWs and has little or no effect on nanowires deep inside a multi-layer.

We have also performed the experiment, where graphene was first applied onto a glass substrate followed by the spray-deposition of AgNWs. This resulted in no enhancement of R_s. We hypothesize that this is because graphene flakes lying flat on the substrate do not have the same ability to efficiently wrap around the wires and engage effectively with the junctions. As shown in Figure 2b, when a dense graphene layer is deposited (at Π = 25 mN m^{-1}), the overall transparency of an electrode can be reduced by as much as ca. 15% thus hindering its use as a transparent electrode. We learned from our previous work on LS deposition of graphene,[26] that the loss in transparency can be avoided by applying lower densities of graphene onto the AgNWs. This can be achieved by reducing the surface pressure during graphene compression. As can be seen in Figure 3d, even though graphene is applied at lower surface pressures (0, 5, and 15 mN m^{-1}) resulting in lower

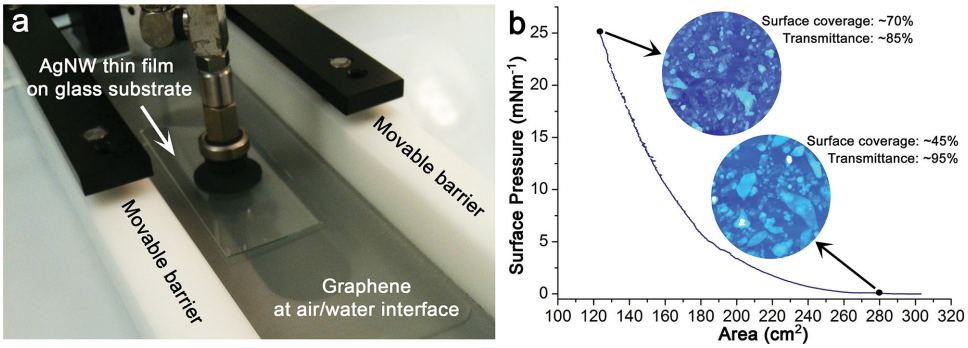

Figure 2. a) A photograph of a Langmuir trough with a dense graphene monolayer deposited onto the water subphase with a glass substrate containing AgNWs above the surface ready for a Langmuir-Schaefer horizontal deposition. b) Representative surface pressure-area (Π-A) isotherm of graphene monolayer at the air-water interface and resulting surface coverage and transmittance of the films deposited at the $\Pi = 25$ mN m^{-1} and $\Pi = 0$ mN m^{-1} (after 3 sequential compression-rarefaction cycles).

surface coverage the percentage improvement in R_s is independent of the surface pressure used. Moreover, by using a low surface pressure ($\approx\Pi = 0$ mN m^{-1}) we find that the deleterious effect of graphene incorporation on T% is minimized while still enhancing conductivity. We also find that using repeated (and reversible) compression of the barriers during preparation of the Langmuir films is necessary to increase homogeneity in graphene distribution meaning more junctions could be covered during deposition.

Using these optimized monolayers, ten different density AgNW networks were wrapped with graphene platelets using LS deposition. As can be seen in **Figure 4**, the electrode transparency due to the presence of graphene was reduced by a maximum of 5%. Although a single layer of graphene is only one atom thick, it absorbs 2.3% of white light.[32] Thus, stacking another layer of graphene on top increases the amount of light absorbed by approximately the same value. Although our fabrication method produces a large population of single-layers, thicker flakes (2, 3 layers as well as multilayers) are also present which explains the changes witnessed.

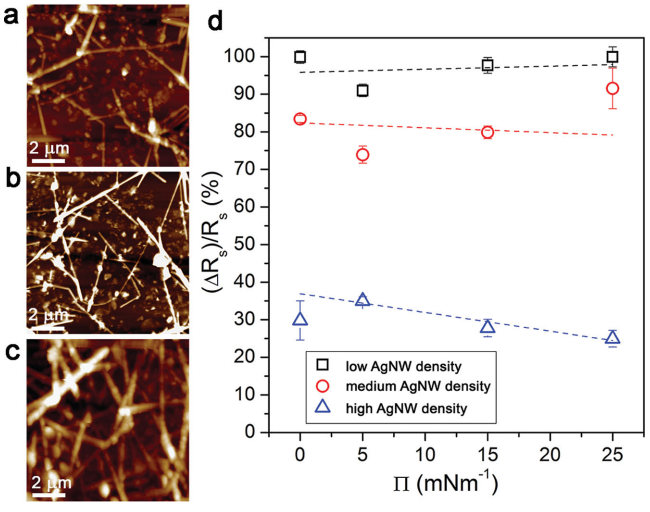

Figure 3. AFM height images of a) L-AgNW, b) M-AgNW, c) H-AgNW networks with graphene blankets wrapped around individual wires deposited using LS deposition technique at $\Pi = 25$ mN m^{-1}. d) The percentage change in R_s of L-AgNW, M-AgNW, and H-AgNW as a function of Π used to deposit graphene flakes on the surface of wires.

Depositing graphene on AgNW layers creates a strong shift toward lower R_s. The shift is particularly strong for lower density AgNW samples where the change can be several orders of magnitude (inset of Figure 4). For example, a L-AgNW sample with an original $R_s = 600$ kΩ/sqr and $T = 97\%$ (corresponding to black square number 1 in Figure 4) is markedly effected due to graphene deposition resulting in values of $R_s = 200$ Ω/sqr and $T = 93\%$ (corresponding to red triangle number 1 in Figure 4) for the resulting hybrid. Similarly, an H-AgNW sample with initial values of R_s of 40 Ω/sqr and $T = 93\%$ (corresponding to black square number 10 in Figure 4) exhibits final values of $R_s = 28.7$ Ω/sqr and $T = 87\%$ (corresponding to red triangle number 10 in Figure 4) after deposition. Current–voltage characteristics of pristine AgNWs and hybrid transparent electrodes exhibit excellent Ohmic behavior regardless of the density of AgNWs and graphene.

It has been reported by Lee et al. that the junction resistance between two wires is on the order of 1Ω.[1] Moreover, the macroscopic resistance in a nanowire ensemble is dominated by the formation of many parallel connections with the lowest resistance connections dominating the macroscopic resistance. It has been suggested for other graphene-like materials that modifications in junction resistance maybe mechanical in origin. Single-layer graphene possesses an intrinsic tensile strength of 130 GPa and in plane Young's modulus of about 1TPa.[33] More importantly, it has the ability to conform to the local environment by bending due to its exceptionally low flexural rigidity.[34–36] The AFM and SEM false color images shown in **Figure 5**a and b appear to support this hypothesis. Wrapping AgNWs by graphene platelets may result in increased wire-to-wire contact. The force exerted by the graphene flakes helps compress the NW network into a more planar structure, reducing the air gap between the wires and consequently reducing wire-wire junction resistance.

When graphene is adsorbed on a metal interface it has been shown both experimentally and computationally that the electronic properties can be altered.[37] This can lead to an enhancement in conduction via "percolation doping"[20] within the hybrid structure. This was first described for polycrystalline graphene films where segregated domains are

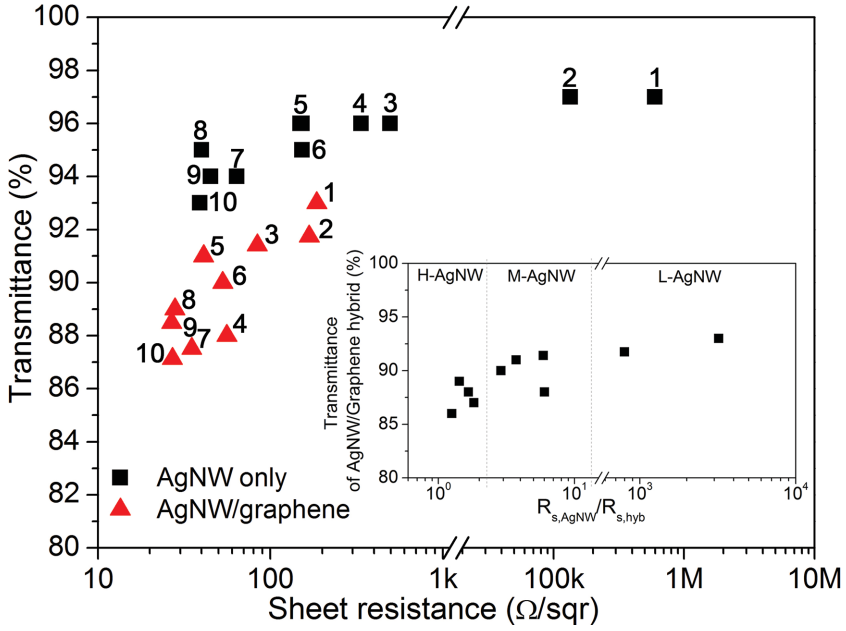

Figure 4. Transmittance plotted versus sheet resistance for (n) pristine AgNW networks and (▲) AgNW/graphene hybrids. Inset: transmittance vs initial R_s of pristine AgNWs ($R_{s,AgNW}$) against Rs of AgNW/graphene hybrid ($R_{s,hyb}$).

connected across grain boundaries by individual AgNWs. Although our hybrid system is the converse situation, the improvement of conductivity is a similar mechanism and can be attributed to the bridging of two AgNWs by graphene platelets, providing additional conduction channels through the network.

This is evidenced by resistance mapping using the SSRM technique. The AFM topography image in **Figure 6**a shows that graphene flakes wrap around the AgNWs. However, not all graphene flakes contribute to the map of current flow when the electrical resistance is measured between the conductive tip and a current collecting back contact (Figure 6b). As resistance is known to scale linearly with graphene thickness the thicker flakes are less conducting and have little impact on the conduction mechanism through the system.[38] Moreover, thicker graphene flakes possess much higher flexural rigidity and thus exhibit greater resistance to bending and weaker connections to the wires. However, as marked by the green circle in Figure 6b and in Supporting Information Figure 2, if a graphene platelet

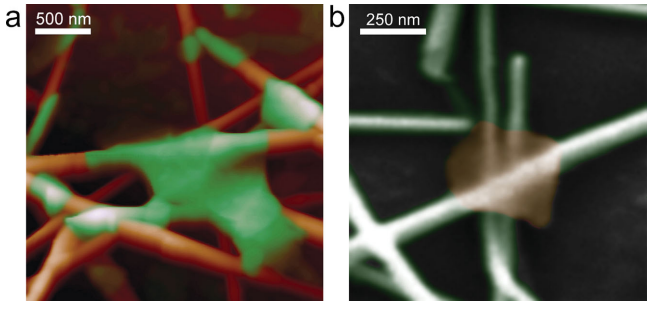

Figure 5. False color a) AFM height image and b) SEM image of graphene-wrapped silver nanowire junctions.

is efficiently bridging between two parallel wires, it provides additional conductive pathways. Although a more quantitative study needs to be carried out using scanning tunneling microscopy, from our analysis, it seems that this bridging phenomenon only occurs for individual layers of graphene.

The extent of the electrical interaction is primarily determined by the work function and the chemical interaction between the graphene lattice and the surface of the metal. We further studied this interaction by measuring the contact potential difference (*CPD*) (Supporting Information Figure 3) of AgNWs, graphene and a combination of both materials deposited on a glass substrate using Kelvin probe force microscopy (KPFM). In general, the *CPD* (V_{CPD}) measured between the probe and the sample is defined as:

$$V_{CPD} = \frac{\phi_{probe} - \phi_{sample}}{-e} \quad (1)$$

where φ_{sample} and φ_{probe} are the work functions of the sample and tip respectively, and e is the electronic charge.[39] The magnitude of the *CPD* is governed by the properties of both the tip and the sample surface. If the AFM probe is separated from the sample surface by a distance d_1, the system is not connected electrically; thus the Fermi levels are of different energies relative to the vacuum level as shown in Figure 6h. When the AFM probe is brought into close proximity to the sample surface, upon electrical connection, the Fermi levels align. Both the probe and the surface of material are now charged (by the formation of an electrcic double layer) (Figure 6i). Due to the charging of the probe and the sample surface, an electrostatic force develops due to the V_{CPD}. This force can then be nullified by applying an external bias (V_{DC}) between the probe and the sample. The magnitude of this bias is a direct measurement of the *CPD* (Figure 6j).

If the sample consists of different materials (in this case glass, AgNWs, graphene, and AgNW/graphene hybrid) and is investigated using exactly the same probe, the potential of the probe can be regarded as the *CPD* reference electrode. Consequently, the map of *CPD* can be directly used to image potential distributions related to local properties of the sample surface.[40] As can be seen in Figure 6, KPFM simultaneously provides information on the sample topography (Figure 6c), phase (Figure 6d) and provides a map of *CPD* (Figure 6e). The *CPD* maps reveal a clear contrast between regions of different electrical interaction. The highest contrast can be seen between the glass and graphene flakes, while the smallest contrast is between the glass and AgNWs. The corresponding height and phase variations are hard to distinguish. The value of *CPD* of AgNWs and graphene on a glass substrate was statistically measured to be 63.6 ± 15.4 mV and 175.3 ± 29.7 mV respectively. The *CPD* of AgNW/graphene hybrid lies between these values (CPD_{hybrid} = 111.5 ± 30.0 mV) (Figure 6f). The work function of graphene is similar to that of graphite, ca. 4.6 eV,

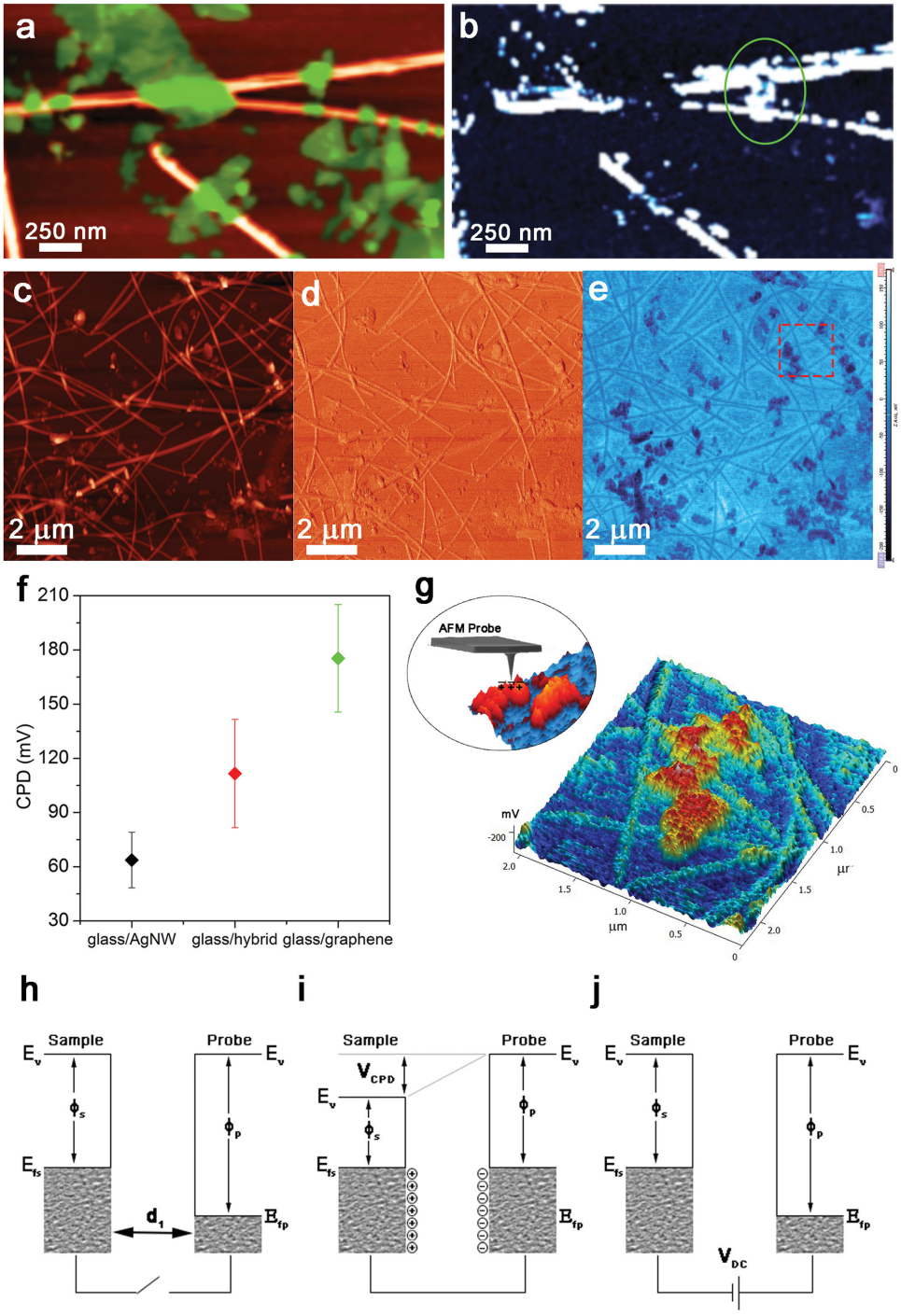

Figure 6. a) AFM topography and b) corresponding SSRM surface conductivity map of L-AgNW with graphene deposited at ≈ $\Pi = 0 mNm^{-1}$. c) AFM d) topography phase and e) simultaneously acquired surface potential map of L-AgNW/graphene hybrid. f) Changes in contact potential difference between the KPFM probe and local surface. g) 3D KPFM surface potential map of an area shown in Figure 6e (Inset: cartoon of formation of electrcic double layer between the probe and the sample surface). Energy diagrams to present the principle of KPFM for h) no electrical contact between the probe and the sample surface, i) Fermi levels of probe and sample have aligned and j) a voltage is applied in order to align the vacuum levels again.

but its exact value depends on the number of layers.[41–43] However, since the work function of Ag is lower than that of graphene (4.3 eV), the graphene is effectively n-type doped as expected from other studies.[41,44]

The above results clearly demonstrate the potential of these hybrid coatings as alternatives to ITO. The finding that for low-density AgNWs coatings, the deposition of graphene produces a ca. 10^5 decrease in resistance is particularly important. Further

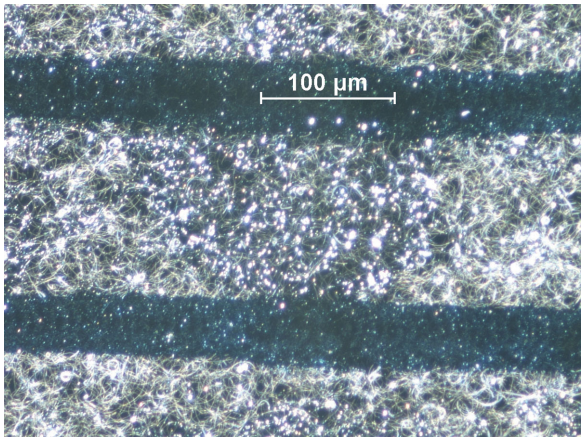

Figure 7. Optical image of a laser ablated regions showing that such process is a feasible process to fabricate touch sensors based on AgNW/graphene hybrids.

optimization of the nanoscale morphology should have major cost saving implications for eventual commercialization. If our hypothesis is correct, an optimized structure would consist of an ensemble of AgNWs deposited at densities corresponding to the onset of percolation with enough graphene deposited so as to bridge junctions across nearest neighbors. Using percolation theory, we can estimate the mass per unit area of AgNWs required to be as low as ≈ 2.6 mg m^{-2} (Supplementary Data 1). This corresponds to more than an order of magnitude reduction in the amount of AgNWs needed to produce a comparable electrode from the raw material.

Finally, we show that it is possible to pattern our hybrid films using a laser ablation process, to produce an electrode array, which is necessary for designing a sensor. In a capacitive display, sensor electrodes detect capacitance changes due to touch. These touch sensors can only be activated by a finger or other conductive object. The sensor area is split up into individual electrodes, each corresponding to a single position. Using laser ablation process, we were able to pattern our hybrid films (**Figure 7**). The resulting scribes are hardly visible to the naked eye and show the same distinguishability to reflected light as a typical ITO sensor.

3. Conclusion

We show that films containing ultra-low density networks of AgNW with sheet resistances in the MΩ regime can undergo significant enhancements to their electrically properties by subsequent deposition of graphene to form hybrids. Using a Langmuir-based technique to deposit pristine graphene platelets on spray deposited silver nanowire networks we have fabricated highly conducting, low cost transparent electrodes. Graphene adsorption at inter-wire junctions as well as graphene connecting adjacent wires can contribute to a marked enhancement in electrical properties by several orders of magnitude. Using our approach the amount of nanowires needed to produce viable transparent electrodes could be more than fifty times less than the equivalent pristine high-density nanowire networks thus having major commercial implications. With touchscreen applications in mind, we show that the resulting films can be patterned using laser ablation to produce electrically isolated scribes necessary for electrode fabrication in touch-sensor devices.

4. Experimental Section

4.1. Fabrication of AgNW Transparent Electrodes

Silver nanowires in isopropyl alcohol were purchased from Seashell Technologies (www.seashelltech.com) (C = 20 mg mL^{-1} as provided by a supplier) and Zejiang Kechuang Advanced Materials Technology Co. Ltd (www.ke-chuang.com) (C = 16 mg mL^{-1} as provided by a supplier). A small volume of the dispersion was diluted down to 0.1 mg/mL with isopropyl alcohol. The average diameter and length of the nanowires were measured to be 40 nm and 14 µm respectively. A large number of samples of low, medium and high-density AgNW films were formed by spraying the diluted dispersions onto glass substrates using an airbrush that was vertically mounted onto a computer controlled hotplate, able to move in the x-y direction.[27]

4.2. Fabrication of Graphene Dispersion

The graphene dispersion was prepared as described elsewhere.[26] Briefly, as-produced sieved graphite powder (Aldrich product 332461, batch number 06106DE) was added to N-methylpyrrolidone (NMP) (spectrophotometric grade, 99.0%) to give an initial graphitic concentration of 10 mg mL^{-1} and was sonicated using a sonic tip (a Sonics VX-750 ultrasonic processor with a flathead tip) for 2 hours. The resulting dispersion was then centrifuged using Hettich Mikro 22R centrifuge for 90 minutes at 1500 rpm. 1 mL of the resulting NMP dispersion (concentration 0.1mg/ml) was mixed with 100 mL of chloroform and sonicated using bath sonicator (fisher scientific FB15051) for 60 minutes, followed by centrifugation (Eppendorf 5702) for 90 minutes at 4000 rpm. The supernatant was then bath sonicated under chilled conditions for a further 30 minutes. The final dispersed graphene concentration in NMP/chloroform mixture was calculated to be ca. 0.007 mg mL^{-1} (as determined by UV–Vis spectrophotometry)

4.3. Fabrication of AgNW/Graphene Hybrids by Langmuir-Schaefer Horizontal Deposition

The Langmuir-Schaefer (LS) deposition of graphene was performed as described elsewhere.[26] Briefly, a commercial NIMA deposition trough (NIMA technology, model 612D) was used. The graphene dispersion in chloroform/NMP mixture prepared as described above was spread onto the water subphase drop-by-drop. The volume of the material deposited ranged from 2 mL to 10 mL depending on the density of graphene layer that needed to be deposited.

The pressure-area isotherms were obtained, after a 10 min waiting time to let the remaining solvent evaporate, at a barrier compression speed of 15 cm^2 min^{-1}. Graphene was then transferred onto the spray-deposited AgNW networks at various surface pressures (Π) ranging from 0 to 25 mNm^{-1} and using a transfer speed of 3 mm/min. Because at Π = 0 mN m^{-1} graphene forms multiple discrete islands, three sequential compression-expansion cycles in the gas phase regime of the Π-A isotherm were performed to increase the packing efficiency of individual graphene flakes.

4.4. Characterization Methods

Surface characterization of the graphene hybrids was performed on a commercial Atomic force microscopy (AFM) system (Ntegra Prima, NT-MDT Co, Russia) using scanning spreading resistance microscopy (SSRM) and single-pass Kelvin probe microscopy (KPM).

AFM topographic and phase-contrast imaging of the graphene hybrids deposited on glass substrates was performed in semi-contact mode with a standard Si cantilever (NSG10) having a spring constant of ca. 11.8 Nm^{-1} and a curvature radius of ca. 9nm. SSRM measurements were used to provide information on the local current (resistance) mapping of the sample. By this method, a conductive metal-coated Si cantilever was used as the top electrode recording current flow between it and the bottom electrode (sample), when a bias voltage was applied. In order to minimize surface damage during scanning and to ensure good contact between the metal-coated tip and sample surface, a Pt-coated cantilever was selected with a spring constant of ca. 2.1 N/m and a radius of curvature of ca. 35 nm (NSG03/Pt, NT-MDT Co, Russia). The contact potential of the hybrid samples was measured by using the single pass KPM technique, where topography and potential distribution are recorded simultaneously. In these KPM measurements, a metal-coated Si cantilever (NSG03/Pt) is oscillated by an ac voltage while the sample remains grounded. In the current AFM studies, all the images were recorded with 512 × 512 pixels in the selected scanning area with a scanning frequency of 1.0 Hz. Before surface characterizations, the AFM scanner in the Ntegra system was precisely calibrated by using a standard grating (TGQ01, NT-MDT Co, Russia). The SEM investigations of composite materials were done using a FEI Quanta scanning electron microscope at an accelerating voltage of 2–5 KeV, a working distance of 8.5 mm. Owing to the good electrical conductivity of the samples, they were imaged without sputtering a metal onto their surface. The current–voltage characteristics have been obtained using a Keithley Model 4200 utilizing two-point probe technique. Prior to the measurement, two opposite edges of the sample were covered with a silver paint acting as contact electrodes. Optical transmission spectra were obtained using a Carry 5000 spectrometer.

4.5. Laser Ablation of the AgNW Films

Using a 1064 nm laser single shot craters were ablated into the film. A pulse energy and a scan speed was similar to the scan speed which would be typically used to scribe ITO in a production environment.

Supporting Information

Supporting Information is available from the Wiley Online Library or from the author.

Acknowledgements

I.J. and A.F. contributed equally to this work. We thank the EPSRC/KTA, Kwan Trust and M-SOLV Ltd. for their financial support of our research activities. We also thank Mrs. Violeta Doukova for general laboratory assistance.

Received: July 29, 2014
Revised: September 1, 2014
Published online: September 26, 2014

[1] J. Lee, S. Connor, Y. Cui, P. Peumans, *Nano Lett.* **2008**, *8*, 689.
[2] J. van de Groep, P. Spinelli, A. Polman, *Nano Lett.* **2012**, *12*, 3138.
[3] C. H. Liu, X. Yu, *Nanoscale Res. Lett.* **2011**, *6*, 75.
[4] S. De, T. M. Higgins, P. E. Lyons, E. M. Doherty, P. N. Nirmalraj, W. J. Blau, J. J. Boland, J. N. Coleman, *ACS Nano* **2009**, *3*, 1767.
[5] K. Cheng, Z. Cui, Q. Li, S. Wang, Z. Du, *Nanotechnology* **2012**, *23*, 425303.
[6] S. Xie, Z. Ouyang, B. Jia, M. Gu, *Opt. Express* **2013**, *21*, A355.
[7] M. S. Miller, J. C. O'Kane, A. Niec, R. S. Carmichael, T. B. Carmichael, *ACS Appl. Mater. Interfaces* **2013**, *5*, 10165.
[8] S. E. Park, S. Kim, D. Y. Lee, E. Kim, J. Hwang, *J. Mater. Chem. A* **2013**, *1*, 14286.
[9] L. Hu, H. Kim, J. Y. Lee, P. Peumans, Y. Cui, *ACS Nano* **2010**, *4*, 2955.
[10] Y. Ahn, Y. Jeong, Y. Lee, *ACS Appl. Mater. Interfaces* **2012**, *4*, 6410.
[11] J. Jiu, M. Nogi, T. Sugahara, T. Tokuno, T. Araki, N. Komoda, K. Suganuma, H. Uchidab, K. Shinozaki, *J. Mater. Chem.* **2012**, *22*, 23561.
[12] C. Preston, Y. Xu, X. Han, J. Munday, L. Hu, *Nano Res.* **2013**, *6*, 461.
[13] T. Araki, J. Jiu, M. Nogi, H. Koga, S. Nagao, T. Sugahara, K. Suganuma, *Nano Res.* **2014**, *7*, 236.
[14] C. Preston, Z. Fang, J. Murray, H. Zhu, J. Dai, J. N. Munday, L. Hu, *J. Mater. Chem. C* **2014**, *2*, 1248.
[15] E. C. Garnett, W. Cai, J. J. Cha, F. Mahmood, S. T. Connor, M. G. Christoforo, Y. Cui, M. D. McGehee, M. L. Brongersma, *Nat. Mater.* **2012**, *11*, 241.
[16] S. Zhu, Y. Gao, B. Hin, J. Li, J. Su, Z. Fan, J. Zhou, *Nanotechnology* **2013**, *24*, 335202.
[17] J. Lee, I. T. S. Kim, J. Y. Lee, *Small* **2013**, *9*, 2887.
[18] T. Tokuno, M. Nogi, J. Jiu, K. Suganuma, *Nanoscale Res. Lett.* **2012**, *7*, 1.
[19] D. Kim, L. Zhu, D. Jeong, K. Chun, Y. Bang, S. Kim, J. Kim, S. Oh, *Carbon* **2013**, *63*, 530.
[20] C. Jeong, P. Nair, M. Khan, M. Lundstrom, M. A. Alam, *Nano Lett.* **2011**, *11*, 5020.
[21] Y. S. Yun, D. H. Kim, B. Kim, H. H. Park, H. J. Jin, *Synth. Met.* **2012**, *162*, 1364.
[22] I. N. Kholmanov, C. W. Magnuson, A. E. Aliev, H. Li, B. Zhang, J. W. Suk, L. L. Zhang, E. Peng, S. H. Mousavi, A. B. Khanikaev, R. Piner, G. Shvets, R. S. Ruoff. *Nano Lett.* **2012**, *12*, 5679.
[23] R. Chen, S. R. Das, C. Jeong, M. R. Khan, D. B. Janes, M. A. Alam, *Adv. Funct. Mater.* **2013**, *23*, 5150.
[24] T. L. Chen, D. S. Ghosh, V. Mkhitaryan, V. Pruneri, *ACS Appl. Mater. Interfaces* **2013**, *5*, 11756.
[25] D. Lee, H. Lee, Y. Ahn, Y. Jeong, D. Lee, Y. Lee, *Nanoscale* **2013**, *5*, 7750.
[26] A. Fahimi, I. Jurewicz, R. J. Smith, C. S. Sharrock, S. J. Henley, J. N. Coleman, A. B. Dalton, *Carbon* **2013**, *64*, 435.
[27] V. Scardaci, R. Coull, P. E. Lyons, D. Rickard, J. N. Coleman, *Small* **2011**, *7*, 2621.
[28] V. Scardaci, R. Coull, J. N. Coleman, L. Byrne, G. Scott, *12th IEEE Conf. Nanotechnology (IEEE-NANO)* **2012**, *1*, 20.
[29] S. De, J. N. Coleman, *MRS Bull.* **2011**, *36*, 774.
[30] S. Sorel, P. E. Lyons, S. De, J. Dickerson, J. N. Coleman, *Nanotechnology* **2012**, *23*, 185201.
[31] P. N. Nirmalraj, P. E. Lyons, S. De, J. N. Coleman, J. J. Boland, *Nano Lett.* **2009**, *9*, 3890.
[32] F. Xia, T. Mueller, Y. Lin, A. Valdes-Garcia, P. Avouris, *Nat. Nanotechnol.* **2009**, *4*, 839.
[33] C. Lee, X. Wei, J. W. Kysar, J. Hone, *Science* **2008**, *321*, 385.
[34] Y. Huang, J. Wu, K. C. Hwang, *Phys. Rev. B* **2006**, *74*, 245413.
[35] J. S. Bunch, M. L. Dunn, *Solid State Commun.* **2012**, *152*, 1359.
[36] S. P. Koenig, N. G. Boddeti, M. L. Dunn, J. S. Bunch, *Nat. Nanotechnol.* **2011**, *6*, 543.
[37] M. Batzill, *Surf. Sci. Rep.* **2012**, *67*, 83.
[38] P. N. Nirmalraj, T. Lutz, S. Kumar, G. S. Duesberg, J. J. Boland, *Nano Lett.* **2010**, *11*, 16.
[39] W. Melitz, J. Shen, A. C. Kummel, S. Lee, *Surf. Sci. Rep.* **2011**, *66*, 1.
[40] J. Lü, E. Delamarche, L. Eng, R. Bennewitz, E. Mayer, H. J. Güntherodt, *Langmuir* **1999**, *15*, 8184.
[41] G. Giovannetti, P. A. Khomyakov, G. Brocks, V. M. Karpan, J. van den Brink, P. J. Kelly, *Phys. Rev. Lett.* **2008**, *101*, 026803.
[42] H. Hibino, H. Kageshima, M. Kotsugi, F. Maeda, F. Z. Guo, Y. Watanabe, *Phys. Rev. B* **2009**, *79*, 125437.
[43] T. Takahashi, H. Tokailin, T. Sagawa, *Phys. Rev. B* **1985**, *32*, 8317.
[44] Y. Ren, S. Chen, W. Cai, Y. Zhu, C. Zhu, R. S. Ruoff, *Appl. Phys. Lett.* **2010**, *97*, 053107.